Contribution from the Laboratory for Molecular Structure and Bonding
and Department of Chemistry, Texas A&M University, College Station, Texas 77843

Synthesis and Structural Characterization of $[n\text{-}Bu_4N]_2[Au_2(i\text{-}MNT)_2]$ (i-MNT = 1,1-Dicyanoethylene-2,2-dithiolate) and Its Oxidative-Addition Products $[Ph_4As]_2[Au_2(i\text{-}MNT)_2Cl_2]$, $[n\text{-}Bu_4N]_2[Au_2(i\text{-}MNT)_2Br_2]$, and $[n\text{-}Bu_4N][Au(i\text{-}MNT)_2]$. Spectral Studies of the Disproportionation of $[n\text{-}Bu_4N]_2[Au_2(i\text{-}MNT)_2X_2]$ ($X = Cl^-$, Br^-, I^-) into $[n\text{-}Bu_4N][AuX_2]$ and $[n\text{-}Bu_4N][Au(i\text{-}MNT)_2]$

Md. Nazrul I. Khan, Suning Wang, and John P. Fackler, Jr.*

Received February 8, 1989

The title compounds have been synthesized and structurally characterized. The short Au···Au distance (2.78 Å) observed between the Au^I centers in $[n\text{-}Bu_4N]_2[Au_2(i\text{-}MNT)_2]$ (**1a**) becomes a strong Au–Au bond (2.550 Å) in the oxidized $[n\text{-}Bu_4N]_2[Au_2(i\text{-}MNT)_2Cl_2]$ (**2**) Au^{II} complex. UV–visible spectral studies of $[n\text{-}Bu_4N]_2[Au_2(i\text{-}MNT)_2X_2]$ [where X = Cl^- (**2**), Br^- (**3**), and I^- (**5**)] show strong absorptions at 550, 586, and 640 nm, respectively. Solution decomposition of $[n\text{-}Bu_4N]_2[Au_2(i\text{-}MNT)_2X_2]$ results in $[n\text{-}Bu_4N][Au(i\text{-}MNT)_2]$ (**4**) and $[n\text{-}Bu_4N][AuX_2]$ by a disproportionation reaction involving rate-limiting kinetics similar to that found in square-planar substitution reactions. Compound **1a** crystallized in the space group $P2_1/c$, with a = 14.228 (3) Å, b = 8.754 (2) Å, c = 20.360 (3) Å, β = 107.49 (1)°, Z = 4, and R = 0.0292. Compound **2** crystallized in the space group $P\bar{1}$, with a = 11.619 (2) Å, b = 12.404 (5) Å, c = 11.108 (2) Å, α = 98.20 (3)°, β = 105.70 (2)°, γ = 110.54 (2)°, Z = 2, and R = 0.0272. Compound **3** crystallized in the space group $C2/c$, with a = 32.18 (2) Å, b = 8.15 (1) Å, c = 21.37 (1) Å, β = 113.48 (5)°, Z = 4, and R = 0.1120. Compound **4** crystallized in the space group $P\bar{1}$, with a = 14.232 (2) Å, b = 16.688 (4) Å, c = 14.213 (2) Å, α = 94.30 (2)°, β = 103.98°, γ = 66.44 (1)°, Z = 2, and R = 0.0407.

Introduction

In recent years, extensive studies have been carried out on dinuclear gold complexes containing either one or two bridging ligands. A number of reviews of this chemistry have been published.[1,2] Special attention has been focused on the oxidative-addition reaction on gold(I) dimers containing anionic bridges such as ylides,[3,4] dialkyldithiocarbamates[5] and dithiophosphinates,[6] and neutral bridging ligands such as (diphenylphosphino)amine[7] and (diphenylphosphino)methane.[8]

The stability of complexes with metal ions in unusually high oxidation states depends on the σ-bonding and π-bonding properties of the ligands. It is well established[4c,9] that metal–metal-bonded Au^{II} complexes bridged by ylide anion ligands are obtained when oxidative-addition reactions are carried out. It is believed that the σ-donor capability of carbon atoms in an ylide ligand and the presence of onium centers adjacent to the four Au–C σ bonds[9a] are responsible for this unexpected stabilization. In the case of sulfur ligands, the ability of sulfur atoms to participate in π bonding as well as σ donation allows the formation of oxidized complexes in which the formal oxidation state of the metal ion can be unusually high.[10] Electron delocalization through the π system on the sulfur ligand[11] appears responsible for the stabilizing influence of these sulfur ligands.

Studies of the oxidative-addition reactions to Au^I dimer complexes containing sulfur bridging ligands have been a subject of interest for several years. In 1981 Burmeister et al.[5d] reported that when the neutral bis(N,N-dialkyldithiocarbamato)digold(I) complexes reacted with Br_2, I_2, $(SCN)_2$, and $(SeCN)_2$ at −78 °C, a dark green solution formed that appeared to contain Au^{II} dimers. Unstable dark green solids were isolated and characterized. These complexes were unstable when the solution was warmed to room temperature; the color quickly became yellow, and the compounds rapidly rearranged to monomeric Au^I and Au^{III} complexes. No structures were obtainable for the green compounds. However, these studies demonstrated that the dithiocarbamate ligands allow the Au^I dimer to be oxidized to a Au^{II} product. Further, these studies suggested that a stable Au^{II} dimer might be formed by halogen oxidation if a stronger σ-donor sulfur ligand were used in the parent Au^I dimer.

We have found that it is possible to form Au^{II} dimer complexes from 1,1-dicyanoethylene-2,2-dithiolate (i-MNT). The sulfur atoms of the dianionic i-MNT ligands are more electron-rich than sulfur atoms in the dithiocarbamate and stabilize the Au^{II} dimers

* To whom correspondence should be addressed.

(1) (a) Uson, R.; Laguna, A. *Coord. Chem. Rev.* **1986**, *70*, 1–50. (b) Melnik, M.; Parish, R. V. *Coord. Chem. Rev.* **1986**, *70*, 157–257. (c) Smith, W. E. *Coord. Chem. Rev.* **1985**, *67*, 311–323.
(2) (a) Mingos, D. M. P. *Gold Bull.* **1984**, *17*, 5–12. (b) Hall, K. P.; Mingos, D. M. P. *Prog. Inorg. Chem.* **1984**, *32*, 237–325. (c) Jones, P. G. *Gold Bull.* **1981**, *14*, 102–118.; **1981**, *14*, 159–166.; **1983**, *16*, 114–124.; **1986**, *19*, 46–57. (d) Braunstein, P.; Rose, J. *Gold Bull.* **1985**, *18*, 17–30.
(3) (a) Schmidbaur, H.; Franke, R. *Angew. Chem., Int. Ed. Engl.* **1973**, *12*, 416; *Inorg. Chim. Acta.* **1975**, *13*, 85–89. (b) Schmidbaur, H.; Jandik, P. *Inorg. Chim. Acta.* **1983**, *74*, 97–99. (c) Schmidbaur, H.; Hartmann, C. *Angew. Chem., Int. Ed. Engl.* **1986**, *25*, 575–577.
(4) (a) Basil, J. D.; Murray, H. H.; Fackler, J. P., Jr.; Tocher, J.; Mazany, A. M.; Trzcinska-Bancroft, B.; Knackel, H.; Dudis, D.; Delord, T. J.; Marler, D. D. *J. Am. Chem. Soc.* **1985**, *107*, 6908. (b) Mazany, A. M.; Fackler, J. P., Jr. *J. Am. Chem. Soc.* **1984**, *106*, 801. (c) Murray, H. H., III; Fackler, J. P., Jr.; Porter, L. C.; Mazany, A. M. *J. Chem. Soc., Chem. Commun.* **1986**, 321–322. (d) Fackler, J. P., Jr.; Porter, L. C. *J. Am. Chem. Soc.* **1986**, *108*, 2750–2751.
(5) (a) Hesse, P.; Jennische, P. *Acta Chim. Scand.* **1972**, 3855. (b) Jennische, P.; Anacker-Eickhoff, H.; Wahlberg, A. *Acta Crystallogr. Sect. A* **1975**, *31*, S143. (c) Kita, H.; Itoh, K.; Tanaka, K.; Tanaka, T. *Bull. Chem. Soc. Jpn.* **1978**, *51*, 3530–3533. (d) Calabro, D. C.; Harrison, B. A.; Palmer, G. T.; Moguel, M. K.; Rebbert, R. L.; Burmeister, J. L. *Inorg. Chem.* **1981**, *20*, 4311–4316.
(6) (a) Kuchen, W.; Mayatepek, H. *Chem. Ber.* **1968**, *101*, 3454. (b) Lauton, S. L.; Rohrbaugh, W. J.; Kokotailo, G. T. *Inorg. Chem.* **1972**, *11*, 2227.
(7) (a) Schmibaur, H.; Wagner, F. E.; Wohllenben-Hammer, A. *Chem. Ber.* **1979**, *112*, 496–500. (b) Uson, R.; Laguna, A.; Laguna, M.; Fraile, M. N.; Jones, P. G.; Sheldrick, G. M. *J. Chem. Soc., Dalton Trans.* **1986**, 291–296.
(8) (a) Uson, R.; Laguna, A.; Laguna, M.; Fernandez, E.; Villacampa, M. D.; Jones, P. G.; Sheldrick, G. M. *J. Chem. Soc., Dalton Trans.* **1983**, 1679–1685. (b) Schmidbaur, H.; Wohllenben, A.; Wagner, F.; Orama, O.; Huttner, G. *Chem. Ber.* **1977**, *110*, 1748–1754. (c) Schmidbaur, H.; Wohllenben, A.; Schubert, U.; Frank, A.; Huttner, G. *Chem. Ber.* **1977**, *110*, 2751–2757.
(9) (a) Schmidbaur, H. *Acc. Chem. Res.* **1975**, *8*, 62. (b) Murray, H. H.; Mazany, A. M.; Fackler, J. P., Jr. *Organometallics* **1975**, *4*, 154. (c) Murray, H. H.; Fackler, J. P., Jr.; Bancroft, B. T. *Organometallics* **1985**, *4*, 1633. (d) Murray, H. H.; Fackler, J. P., Jr.; Tocher, D. A. *J. Chem. Soc., Chem. Commun.* **1985**, 1278. (e) Knackel, K. C.; Dudis, D. S.; Fackler, J. P., Jr. *Organometallics* **1984**, *3*, 1312. (f) Murray, H. H.; Fackler, J. P., Jr.; Mazany, A. M.; Porter, L. C.; Shain, L.; Falvello, L. R. *Inorg. Chim. Acta* **1986**, *114*, 171. (g) Fackler, J. P., Jr.; Murray, H. H.; Basil, J. D. *Organometallics* **1984**, *3*, 821. (h) Schmidbaur, H.; Hartmann, C.; riete, J.; Huber, B.; Muller, G. *Organometallics* **1986**, *5*, 1652.
(10) Schmidbaur, H.; Dask, C. K. *Adv. Inorg. Chem. Radiochem.* **1982**, *25*, 239.

0020-1669/89/1328-3579$01.50/0

sufficiently to allow their isolation and X-ray characterization. A number of reviews have appeared on the 1,1-dithiolato complexes[11b,12] of various metal ions; however, there has been no report of the $[Au^{I}_2(i\text{-}MNT)_2]^{2-}$ anion. The complexes $[Y^+]_2[Au^{I}_2(i\text{-}MNT)_2]^{2-}$ (where $Y^+ = n\text{-}Bu_4N$ or Ph_4As) has been synthesized, and reactions with halogens have been carried out. A communication describing some of these results has appeared.[13] Here we present the detailed X-ray characterization of these complexes and kinetic studies of the disproportionation reaction in solution of the oxidized Au^{II} products as studied by UV–visible spectroscopy.

Experimental Section

All reactions were carried out in oven-dried Schlenk glassware by using standard inert-atmosphere techniques. Tetrahydrofuran was distilled from sodium (metal)/benzophenone and acetonitrile was distilled from P_4O_{10} before use. All ^1H NMR spectra were obtained in CD_3CN at 200 MHz with a Varian XL-200 spectrometer at 25 °C using internal Me_4Si as a standard. All infrared spectra were recorded as Nujol mulls on a Perkin-Elmer 783 spectrometer at 20 °C using CsI or KBr (200–4000 cm^{-1}) plates. UV–visible studies were carried out on a Cary 17 spectrophotometer. Microanalyses were performed by Galbraith Laboratories Inc. or Desert Analytics. The compound $[Au_2(PPh_3)_2S_2CC(CN)_2]$, bis(triphenylphosphine)(1,1-dicyanoethylene-2,2-dithiolato)digold(I), was prepared according to the procedure reported.[14]

Preparation of $[Y^+]_2[Au_2(i\text{-}MNT)_2]$ (1a–c, $Y^+ = [n\text{-}Bu_4N]^+$, K^+, Ph_4As). Method A. To a stirred suspension of 0.20 g (0.19 mmol) of $[Au_2(PPh_3)_2(i\text{-}MNT)]$ in CH_3CN (8 mL) was added 0.04 g (0.19 mmol) of $K_2(i\text{-}MNT)$. The colorless solid immediately dissolved to give a yellow solution. The solution was stirred for 5 h at room temperature, after which 2 equiv of either $n\text{-}Bu_4NCl$ or Ph_4AsCl was added in one portion. In both cases immediate precipitation of KCl was observed. The mixture was stirred for 1 h. The KCl was separated by filtration. For the $n\text{-}Bu_4NCl$ reaction the volume of solution was reduced by half under high vacuum, and then dry diethyl ether was added until no additional precipitate formed. A light yellow crystalline solid (0.164 g, ~75% yield) was obtained from the yellow solution after standing overnight in the freezer. For the Ph_4AsCl reaction an orange solid (0.231 g, ~85%) was obtained by addition of diethyl ether. IR: ν_{CN} for $[n\text{-}Bu_4N]_2[Au_2(i\text{-}MNT)_2]$ 2200 cm^{-1}. The compound melts at 173 °C. Anal. Calcd for $C_{40}H_{72}A_{42}N_6S_4$: C, 41.46; H, 6.21; N, 7.25. Found: C, 41.72; H, 6.03; N, 7.15.

Method B. The compounds $[n\text{-}Bu_4N]_2[Au_2(i\text{-}MNT)_2]$ (**1a**) in 80% yield and $[Ph_4As]_2[Au_2(i\text{-}MNT)_2]$ (**1c**) in 85% yield were obtained from a reaction between $K_2[Au_2(i\text{-}MNT)_2]$ and $n\text{-}Bu_4NCl$ or Ph_4AsCl, respectively, in CH_2Cl_2 at room temperature.

Method C. The compound $K_2[Au_2(i\text{-}MNT)_2]$ (**1b**) was obtained as a red solid in 60% yield from the yellow CH_3CN solution in method A by addition of diethyl ether.

Preparation of $[Ph_4As]_2[Au_2(i\text{-}MNT)_2Cl_2]$ (2). A 20-mg amount (0.014 mmol) of $[Ph_4As]_2[Au_2(i\text{-}MNT)_2]$ was dissolved in a mixture of CH_3CN (1 mL) (or CH_2Cl_2) and THF (5 mL) at room temperature. While this colorless solution was stirred at −78 °C, 4.21 mg (0.015 mmol) of $C_6H_5ICl_2$ was added in one portion under an inert atmosphere. An immediate reaction was observed with the appearance of a deep green color that changed to purple within 5–8 min. After being stirred for 20 min at −78 °C, the solution was deep purple. Dry Et_2O (~2 mL) was added at −78 °C to the solution in small portions until a purple solid appeared temporarily. The solution was placed in a freezer. A crystalline purple solid (14.59 mg, ~70%) separated after 7 days at −20 °C. IR: ν_{CN} 2200 (s) cm^{-1}. Mp: 191–192 °C. Anal. Calcd for $C_{56}H_{40}As_2Au_2Cl_2N_4S_4$: C, 44.50; H, 2.64; N, 3.71. Found: C, 44.57; H, 2.61; N, 3.69.

Preparation of $[n\text{-}Bu_4N]_2[Au_2(i\text{-}MNT)_2Br_2]$ (3). A few drops of Br_2 (in CCl_4) were added to a stirred solution of $[n\text{-}Bu_4N]_2[Au_2(i\text{-}MNT)_2]$ (20 mg, ~0.017 mmol) in a mixture of CH_3CN or CH_2Cl_2 (1 mL) and THF (5 mL) at −78 °C. A deep dark green crystalline solid (11.37 mg, ~50% yield) separated when the solution with a small amount of Et_2O was stored at −20 °C for 5 days. IR: ν_{CN} 2200 cm^{-1}. Mp: 94 °C dec. Anal. Calcd for $C_{40}H_{72}Au_2Br_2N_6S_4$: C, 36.44; H, 5.46. Found: C, 36.86; H, 5.73.

Preparation of $[n\text{-}Bu_4N][Au(i\text{-}MNT)_2]$ (4). A deep green solution of **3** in CH_2Cl_2 (3 mL) was allowed to warm to room temperature. Within a few minutes the solution changed to light yellow. Addition of Et_2O (2 mL) gave red crystalline solid **4** after 7 days at 20 °C. Light yellow needle-shaped crystals also were obtained. The yellow crystals are $[n\text{-}Bu_4N][AuBr_2]$, the other decomposition product.

UV–Visible Spectra. A 2.6-mg amount (2.0×10^{-3} mmol) of the green solid $[n\text{-}Bu_4N]_2[Au_2(i\text{-}MNT)_2Br_2]$ (**3**) was dissolved in 4 mL of CH_3CN in a 1-mm square quartz cell at room temperature, giving a 5×10^{-4} M solution.

A 2.8-mg amount (1.9×10^{-3} mmol) of $[Ph_4As]_2[Au_2(i\text{-}MNT)_2]$ (**1c**) was dissolved in 4 mL of CH_3CN in a 1-mm square quartz cell at room temperature. To this was added 0.55 mg (1.9×10^{-3} mmol) of $C_6H_5ICl_2$, giving a 5×10^{-4} M solution of $[Ph_4As]_2[Au_2(i\text{-}MNT)_2Cl_2]$ (**2**).

A 20-mg amount (0.014 mmol) of $[Ph_4As]_2[Au_2(i\text{-}MNT)_2]$ (**1c**) was dissolved in CH_3CN (4 mL) in the cell. To this was added 0.50 mg (1.9×10^{-3} mmol) of I_2, giving a 5×10^{-4} M solution of $[Ph_4As]_2[Au_2(i\text{-}MNT)_2I_2]$ (**5**).

For variable-temperature measurements a special cell holder was used. The cell temperature was maintained at the required temperature by thermostated control. For each complex, spectra were recorded at three different temperatures as a function of time. For each temperature run a fresh sample was prepared.

X-ray Diffraction Analysis. Light yellow crystals of $[Bu_4N]_2[Au_2(i\text{-}MNT)_2]$ (**1a**) suitable for X-ray diffraction analysis were grown by slow evaporation of the mixed solvents CH_2Cl_2/diethyl ether at 20 °C. The dark purple crystals of $[Ph_4As]_2[Au_2(i\text{-}MNT)_2Cl_2]$ (**2**) and dark green crystals of $[n\text{-}Bu_4N]_2[Au_2(i\text{-}MNT)_2Br_2]$ (**3**) were obtained by crystallization in 60% THF/40% ether at −20 °C. The red crystals of $[n\text{-}Bu_4N][Au(i\text{-}MNT)_2]$ (**4**) were grown by slow evaporation of the mixed solvents CH_2Cl_2/ether at 20 °C. Crystals were mounted on glass fibers with epoxy cement. Unit cells were determined from 25 machine-centered reflections obtained from rotation photographs. Data were collected on a Nicolet R3m/E diffractometer controlled by a Data General Nova 4 minicomputer using Mo Kα radiation at ambient temperature over the range of $3 < 2\theta < 45°$ for all compounds.

The data were corrected for decay, absorption, Lorentz, and polarization effects. All data processing was performed on a Data General Eclipse S140 minicomputer using the SHELTL crystallographic computational package (version 4.1 for **1a**, **2**, and **3**, version 5.1 for **4**).

The compounds **2** and **4** crystallize in $P\bar{1}$ space group. The space group $P2_1/c$ for **1a** was established uniquely from the systematic absences. The systematic absences hkl, $h + k = 2n + 1$, and $h0l$, $l = 2n + 1$, observed for compound **3** are consistent with the space group $C2/c$ or Cc. The former was determined by the successful solution and refinement of the structure. The metal atoms positions in **1a**, **2**, and **4** were determined by heavy-atom methods, while the metal atom position in **3** was located by direct methods. All remaining non-hydrogen atoms were obtained from subsequent difference Fourier maps. All non-hydrogen atoms in **1a** and **2** were refined anisotropically. Atoms heavier than a carbon atom in **3** were refined anisotropically. Only gold and sulfur atoms in **4** were refined anisotropically. Hydrogen atoms on the *n*-butyl groups in **1a**, **3**, and **4** and on the phenyl rings in **2** were calculated by using fixed C–H bond lengths, 0.96 Å. Their contributions were included in the structure factor calculations. Two independent molecules in the crystals of **4** were found in the unit cell and refined independently. Crystals of compound **3** were partially twinned, which could have caused the high R values of the structure. The data for crystallographic analysis of all the compounds are given in Table I.

Results and Discussion

The compound $[Y^+]_2[Au_2(i\text{-}MNT)_2]$ (**1**) was obtained as a stable dinuclear Au^I complex in approximately 80% yield. With PPh_3AuCl as a starting material, either of two synthetic routes can be used: (1) a one-step reaction with 2 or more equiv of $K_2(i\text{-}MNT)$ in 12–24 h gave only compound **1**, yield 60%; (2) a two-step reaction involving formation of $[Au_2(PPh_3)_2(i\text{-}MNT)]$[14] followed by reaction with 1 equiv of $K_2i\text{-}MNT$ gave $[Y^+]_2[Au_2(i\text{-}MNT)_2]$ in a high (>80%) yield. It was observed that various counterions have little effect on these complexes except for differences in solubility. Complexes with Ph_4As and PPN as counterions show considerable solubility, and reactions are easily studied. The IR spectrum shows ν_{CN} stretching frequencies at 2190 (s) and 2200 (sh) cm^{-1}, indicating the presence of *i*-MNT ligands. The various complexes were stable at room temperature in both solid and solution.

(11) (a) Gray, H. B. *Transition Metal Chemistry*; Carlin, R. L., Ed.; Marcel Dekker: New York, 1965; Vol. 1, 240. (b) Burns, R. P.; McCullough, F. P.; McAuliffe, C. A. *Adv. Inorg. Chem. Radiochem.* **1980**, *23*, 211.
(12) (a) Coucouvanis, D. *Prog. Inorg. Chem.* **1970**, *11*, 232. (b) Coucouvanis, D. *Prog. Inorg. Chem.* **1979**, *26*, 301.
(13) Khan, M. N. I.; Fackler, J. P., Jr.; King, C.; Wang, J. C.; Wang, S. *Inorg. Chem.* **1988**, *27*, 1672.
(14) Khan, M. N. I.; Wang, S.; Heinrich, D. D.; Fackler, J. P., Jr. *Acta Crystallogr., Sect. C* **1988**, *C44*, 822.

Table I. Crystallographic Data for **1a–4**

	1a	2	3	4
formula	$C_{40}H_{72}Au_2N_6S_4$	$C_{56}H_{40}Au_2N_4As_2Cl_2$	$C_{40}H_{72}Au_2N_6S_4Br_2$	$C_{24}H_{36}AuN_5S_4$
a, Å	14.228 (3)	11.619 (2)	32.18 (2)	14.232 (2)
b, Å	8.754 (2)	12.404 (5)	8.15 (1)	16.688 (4)
c, Å	20.360 (3)	11.108 (2)	21.37 (1)	14.231 (2)
α, deg	90.000	98.20 (3)	90.000	94.30 (2)
β, deg	107.49 (1)	105.70 (2)	113.48 (5)	103.98 (1)
γ, deg	90.000	110.54 (2)	90.000	66.44 (1)
V, Å^3	2418.5 (8)	1372.3 (7)	5140 (5)	3002.2 (9)
Z	2	1	4	4
fw	1157.4	1510.8	1317.8	719.21
space group	$P2_1/c$	$P\bar{1}$	$C2/c$	$P\bar{1}$
temp, °C	22	22	22	22
radiation	graphite-monochromated Mo Kα (λ = 0.710 73 Å)			
d_{calc}, g/cm^3	1.59	1.80	1.70	0.80
μ(Mo Kα), cm^{-1}	64.1	67.11	76.8	25.7
transm factors: max; min	0.783; 0.519	0.970; 0.405	0.939; 0.492	0.940; 0.558
R^a	0.0292	0.0272	0.1120	0.0407
$R_w{}^b$	0.0304	0.0282	0.1062	0.0398
g	0.002 09	0.000 57	0.001 51	0.000 46

$^a R = \sum||F_o| - |F_c||/\sum|F_o|$. $^b R_w = [\sum w^{1/2}(|F_o| - |F_c|)]/\sum w^{1/2}|F_o|$; $w^{-1} = [\sigma^2(|F_o|) + |g|F_o^2]$.

Oxidative-Addition Reactions. It has been suggested[15] that oxidative addition to metal systems with a d^{10} electron configuration (ionic metal atom model) first requires electronic promotion from the d^{10} atomic configuration to the s^1d^9 configuration. In the d^{10} configuration for Au^I all five 5d orbitals are doubly occupied. However, the d^9s^1 configuration can form singly occupied ds-hybridized orbitals capable of forming covalent bonds to an incoming ligand or to another metal center. For free atomic Pd^0, spectroscopy places the d^9s^1 state 22 kcal/mol higher than the d^{10} state, while for atomic Pt^0 the d^9s^1 state is 11 kcal/mol below the d^{10} state. Assuming ligands stabilize the d^{10} ground state a comparable amount in each metal center, oxidative addition to Pt^0 complexes is expected to be more favorable than to Pd^0 complexes.

In the case of complexes wherein the closed-shell d^{10} electronic configuration best describes the ion or atom, some mixing with the higher s and p levels is expected. The nearly linear geometry generally found for the ligand arrangement in Au^I complexes appears to be caused by mixing with only one of the three p levels, the other two being significantly higher in energy. This p-orbital splitting is not nearly as pronounced when relativistic effects[16] are smaller such as for Pd^0 which more readily forms tetrahedral PdL_4 complexes than does Au^I. Inspite of this difference of coordination the ease of oxidative addition appears to relate to the atomic separation of d^{10} from d^9s^1.

This ease of formation of the "open-shell" d^9s^1 configuration also depends on the electron-donating ability of the ligands (and their π acidity). Strong σ-donating ligands such as those bonding through C are expected to support oxidative addition relative to reactions with complexes containing weaker σ-donating and stronger π-accepting ligands. Oxidative addition to gold(I) ylide dimers occurs readily but $[Au^I(dppm)]_2^{2+}$, dppm = $(Ph_2P)_2CH_2$, does not add even strong oxidants such as Cl_2. The increased overall charge in the cationic complex undoubtedly also stabilizes the closed-shell structure.

The gold(I) dithiocarbamate[5d] dimer is structurally similar to the ylide dimer, but it undergoes oxidative addition much less readily and the Au^{II} product is less stable. The sulfur atoms have both σ-donor and π-acceptor properties.

Unlike the neutral dithiocarbamate dimer[5d] the i-MNT dimers are dianionic. The extra electron density on the gold centers makes oxidative addition more favorable and leads to stable dimeric Au^{II} complexes. It must be pointed out, however, that no oxidative-addition products have been observed to date with sulfur coordinating ligands when the oxidant is an alkyl halide although many have been observed with the gold(I) ylide dimers.

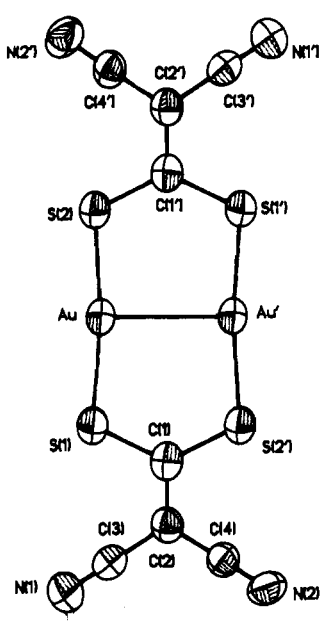

Figure 1. ORTEP drawing of the molecular structure and labeling scheme for the anion portions of compound **1a**. Cation portions are omitted for clarity.

A series of oxidative-addition reactions on $[Y^+]_2[Au_2(i\text{-}MNT)_2]$ with halogens were carried out at −78 °C in various solvent systems such as THF, CH_2Cl_2, and a mixture of THF/CH_3CN and CH_2Cl_2/CH_3CN. The reactions were found to be independent of solvent systems. These reactions have produced $[Y^+]_2[Au_2(i\text{-}MNT)_2X_2]$ [X = Cl^- (purple), Br^- (green), I^- (green)] complexes. These compounds also can be made at room temperature, but decomposition to a yellow solution is rapid. In solution the purple and green compounds are found to be light and temperature sensitive.

The relative stability of these compounds in solutions at room and low temperature is Cl > Br ≫ I. Upon precipitation by addition of Et_2O, **2** and **3** appear to be relatively stable under an inert atmosphere even at room temperature; however, a very slow decomposition for **2** was observed. At low temperature, they can be stored for several weeks. In the case of I_2, we were not able to obtain $[Y^+]_2[Au_2(i\text{-}MNT)_2I_2]$ (**5**) as a solid. IR spectra of **2** and **3** as solids showed the CN stretching frequency at 2200 (s) cm^{-1}, indicating the presence of the i-MNT ligands.

As described above, **2** and **3** in solution decompose to a yellow solution. This yellow solution was found to contain $[n\text{-}Bu_4N][Au(i\text{-}MNT)_2]$ (**4**) and $[n\text{-}Bu_4N][AuX_2]$ upon diethyl ether ad-

(15) Low, J. J.; Goddard, W. A. *Organometallics* **1986**, *5*, 609.
(16) Pyykkö, P. *Chem. Rev.* **1988**, *88*, 563–594.
(17) Khan, M. N. I.; King, C.; Heinrich, D. D.; Fackler, J. P., Jr.; Porter, L. C. *Inorg. Chem.*, in press.

Table II. Atomic Coordinates (×10⁴) and Isotropic Thermal Parameters (Å² × 10³)[a] for $[n\text{-Bu}_4\text{N}]_2[\text{Au}_2(i\text{-MNT})_2]$ (**1a**)

atom	x	y	z	U_{iso}[b]
Au	4752 (1)	5350 (1)	5599 (1)	48 (1)*
S(1)	6288 (2)	4817 (3)	6327 (1)	68 (1)*
S(2)	3160 (2)	5957 (3)	5002 (1)	56 (1)*
N(1)	8502 (6)	3582 (12)	7607 (4)	94 (4)*
N	2397 (4)	3887 (7)	770 (3)	40 (2)*
N(2)	9166 (5)	2091 (10)	5774 (4)	81 (4)*
C(1)	7058 (6)	4097 (9)	5880 (4)	49 (3)*
C(2)	7935 (5)	3481 (9)	6275 (4)	52 (3)*
C(3)	8249 (6)	3519 (11)	7026 (5)	64 (4)*
C(4)	8614 (6)	2730 (10)	5988 (4)	55 (3)*
C(11)	2529 (5)	2661 (9)	1330 (4)	52 (3)*
C(12)	1815 (5)	2754 (10)	1754 (4)	60 (4)*
C(13)	2106 (7)	1656 (12)	2353 (4)	75 (4)*
C(14)	1384 (8)	1639 (16)	2757 (5)	107 (6)*
C(21)	1356 (4)	3782 (9)	254 (3)	43 (3)*
C(22)	1106 (5)	2358 (10)	−161 (4)	55 (3)*
C(23)	69 (5)	2495 (11)	−673 (4)	60 (4)*
C(24)	−262 (7)	1056 (13)	−1089 (6)	94 (5)*
C(31)	2511 (5)	5498 (9)	1066 (4)	47 (3)*
C(32)	3487 (5)	5855 (10)	1599 (4)	59 (3)*
C(33)	3531 (6)	7492 (10)	1823 (4)	61 (4)*
C(34)	4530 (7)	7922 (12)	2334 (5)	84 (5)*
C(41)	3169 (5)	3551 (8)	410 (4)	42 (3)*
C(42)	3188 (6)	4671 (9)	−161 (4)	56 (3)*
C(43)	3812 (6)	4052 (10)	−585 (4)	59 (3)*
C(44)	3919 (7)	5182 (11)	−1117 (5)	78 (4)*

[a] Estimated standard deviations in the least significant digits are given in parentheses. [b] For values with asterisks, the equivalent isotropic U is defined as one-third of the trace of the $\mathbf{U}_{ij}$ tensor.

Table III. Bond Lengths (Å)[a] for $[n\text{-Bu}_4\text{N}]_2[\text{Au}_2(i\text{-MNT})_2]$ (**1a**)

Au–S(1)	2.283 (2)	Au–S(2)	2.280 (2)
Au–Au(a)	2.796 (1)	S(1)–C(1)	1.735 (9)
S(2)–C(1a)	1.727 (8)	N(1)–C(3)	1.129 (13)
N–C(11)	1.534 (10)	N–C(21)	1.535 (7)
N–C(31)	1.521 (10)	N–C(41)	1.516 (10)
N(2)–C(4)	1.149 (12)	C(1)–C(2)	1.372 (10)
C(1)–S(2a)	1.727 (8)	C(2)–C(3)	1.455 (12)
C(2)–C(4)	1.427 (13)	C(11)–C(12)	1.514 (13)
C(12)–C(13)	1.508 (12)	C(13)–C(14)	1.492 (16)
C(21)–C(22)	1.485 (11)	C(22)–C(23)	1.530 (9)
C(23)–C(24)	1.510 (14)	C(31)–C(32)	1.512 (9)
C(32)–C(33)	1.497 (12)	C(33)–C(34)	1.531 (11)
C(41)–C(42)	1.525 (11)	C(42)–C(43)	1.508 (13)
C(43)–C(44)	1.505 (14)		

[a] Estimated standard deviations in the least significant digits are given in parentheses.

Table IV. Bond Angles (deg)[a] for $[n\text{-Bu}_4\text{N}]_2[\text{Au}_2(i\text{-MNT})_2]$ (**1a**)

S(1)–Au–S(2)	172.2 (1)	S(1)–Au–Au(a)	94.6 (1)
S(2)–Au–Au(a)	93.2 (1)	Au–S(1)–C(1)	111.2 (2)
Au–S(2)–C(1a)	112.7 (3)	C(11)–N–C(21)	110.1 (5)
C(11)–N–C(31)	112.2 (5)	C(21)–N–C(31)	106.9 (5)
C(11)–N–C(41)	106.2 (5)	C(21)–N–C(41)	110.1 (5)
C(31)–N–C(41)	111.3 (5)	S(1)–C(1)–C(2)	116.0 (6)
S(1)–C(1)–S(2a)	127.5 (4)	C(2)–C(1)–S(2a)	116.4 (7)
C(1)–C(2)–C(3)	122.9 (8)	C(1)–C(2)–C(4)	123.1 (7)
C(3)–C(2)–C(4)	114.1 (7)	N(1)–C(3)–C(2)	178.4 (11)
N(2)–C(4)–C(2)	177.8 (9)	N–C(11)–C(12)	115.6 (6)
C(11)–C(12)–C(13)	111.0 (7)	C(12)–C(13)–C(14)	112.6 (8)
N–C(21)–C(22)	117.0 (6)	C(21)C(22)–C(23)	109.7 (6)
C(22)–C(23)–C(24)	112.9 (7)	N–C(31)–C(32)	116.1 (6)
C(31)–C(32)–C(33)	111.1 (6)	C(32)–C(33)–C(34)	112.7 (7)
N–C(41)–C(42)	115.0 (6)	C(41)–C(42)–C(43)	110.6 (7)
C(42)–C(43)–C(44)	112.2 (8)		

[a] Estimated standard deviations in the least significant digits are given in parentheses.

dition. The compound $[n\text{-Bu}_4\text{N}][\text{Au}(i\text{-MNT})_2]$ was isolated as deep red crystals and has been structurally characterized. A similar decomposition of $[\text{Au}^{\text{II}}_2(\text{S}_2\text{CNEt}_2)_2\text{X}_2]$ was reported[5d] to give $[\text{AuX}_2][\text{Au}(\text{S}_2\text{CNEt}_2)_2]$ as a stable solid product.

Table V. Atomic Coordinates (×10⁴) and Isotropic Thermal Parameters (Å² × 10³)[a] for $[\text{Ph}_4\text{As}]_2[\text{Au}_2(i\text{-MNT})_2\text{Cl}_2]$ (**2**)

atom	x	y	z	U_{iso}[b]
Au	629 (1)	300 (1)	4237 (1)	41 (1)*
As	5743 (1)	1947 (1)	−1505 (1)	44 (1)*
S(1)	1580 (2)	2298 (2)	5236 (2)	75 (1)*
S(2)	104 (2)	1586 (2)	7048 (2)	79 (1)*
Cl	1847 (2)	859 (2)	2847 (2)	78 (1)*
C(1)	1104 (6)	2628 (6)	6525 (6)	47 (3)*
C(2)	1577 (8)	3817 (7)	7182 (7)	62 (4)*
C(3)	1244 (9)	4164 (7)	8280 (8)	81 (4)*
C(4)	2420 (11)	4730 (8)	6811 (9)	96 (6)*
N(1)	972 (10)	4469 (8)	9136 (9)	125 (6)*
N(2)	3134 (12)	5495 (8)	6556 (10)	145 (7)*
C(11)	4535 (7)	2188 (6)	−726 (6)	49 (3)*
C(12)	4848 (8)	3325 (7)	−22 (8)	72 (4)*
C(13)	4022 (9)	3500 (8)	613 (9)	84 (5)*
C(14)	2915 (9)	2569 (9)	506 (9)	85 (6)*
C(15)	2622 (8)	1459 (8)	−196 (9)	82 (5)*
C(16)	3412 (7)	1249 (7)	−832 (8)	64 (4)*
C(21)	4911 (6)	424 (6)	−2723 (7)	50 (3)*
C(22)	5206 (7)	−513 (6)	−2430 (7)	61 (4)*
C(23)	4575 (9)	−1620 (7)	−3305 (8)	76 (5)*
C(24)	3658 (9)	−1798 (8)	−4453 (9)	78 (5)*
C(25)	3374 (9)	−873 (9)	−4777 (8)	92 (5)*
C(26)	4010 (8)	256 (7)	−3905 (7)	74 (4)*
C(31)	6274 (8)	3214 (6)	−2302 (6)	52 (4)*
C(32)	7587 (9)	3865 (7)	−2062 (7)	70 (4)*
C(33)	7948 (11)	4792 (9)	−2620 (10)	101 (6)*
C(34)	7027 (15)	5077 (9)	−3401 (10)	103 (7)*
C(35)	5707 (13)	4429 (11)	−3594 (10)	109 (7)*
C(36)	5357 (10)	3513 (9)	−3052 (8)	82 (5)*
C(41)	7234 (6)	2001 (5)	−185 (6)	42 (3)*
C(42)	8166 (7)	1724 (7)	−550 (7)	62 (4)*
C(43)	9242 (8)	1761 (8)	382 (9)	78 (5)*
C(44)	9357 (8)	2067 (7)	1665 (9)	76 (4)*
C(45)	8444 (8)	2348 (7)	2022 (7)	76 (4)*
C(46)	7363 (7)	2301 (6)	1094 (6)	57 (4)*

[a] Estimated standard deviations in the least significant digits are given in parentheses. [b] For values with asterisks, the equivalent isotropic U is defined as one-third of the trace of the $\mathbf{U}_{ij}$ tensor.

Table VI. Bond Lengths (Å)[a] for $[\text{Ph}_4\text{As}]_2[\text{Au}_2(i\text{-MNT})_2\text{Cl}_2]$ (**2**)

Au–S(1)	2.286 (2)	Au–Cl	2.380 (3)
Au–Au(a)	2.550 (1)	Au–S(2a)	2.287 (2)
As–C(11)	1.919 (9)	As–C(21)	1.902 (6)
As–C(31)	1.909 (8)	As–C(41)	1.916 (6)
S(1)–C(1)	1.716 (8)	S(2)–C(1)	1.699 (7)
S(2)–Au(a)	2.287 (2)	C(1)–C(2)	1.384 (10)
C(2)–C(3)	1.431 (14)	C(2)–C(4)	1.409 (13)
C(3)–N(1)	1.136 (16)	C(4)–N(2)	1.149 (15)
C(11)–C(12)	1.380 (11)	C(11)–C(16)	1.373 (10)
C(12)–C(13)	1.391 (16)	C(13)–C(14)	1.356 (13)
C(14)–C(15)	1.357 (15)	C(15)–C(16)	1.370 (15)
C(21)–C(22)	1.378 (12)	C(21)–C(26)	1.375 (10)
C(22)–C(23)	1.377 (10)	C(23)–C(24)	1.352 (12)
C(24)–C(25)	1.369 (16)	C(25)–C(26)	1.394 (11)
C(31)–C(32)	1.380 (12)	C(31)–C(36)	1.361 (14)
C(32)–C(33)	1.374 (14)	C(33)–C(34)	1.368 (19)
C(34)–C(35)	1.397 (20)	C(35)–C(36)	1.350 (17)
C(41)–C(42)	1.384 (12)	C(41)–C(46)	1.369 (10)
C(42)–C(43)	1.372 (12)	C(43)–C(44)	1.379 (14)
C(44)–C(45)	1.360 (15)	C(45)–C(46)	1.369 (11)

[a] Estimated standard deviations in the least significant digits are given in parentheses.

Description of the Structures. Bond distances, angles, and thermal and positional parameters for compounds **1a–4** are given in Tables II–IV, V–VII, VIII–X, and XI–XIII, respectively.

The molecular structure of **1a** is shown in Figure 1. The anion portion of this molecule is nearly planar. The two gold atoms are bridged by two *i*-MNT ligands by bonding through the sulfur atoms, Au–S(1) = 2.283 (2) Å and Au–S(2) = 2.280 (2) Å. The coordination of the sulfur atoms to the Au^{I} center is linear, S(1)–Au–S(2)′ = 172.2 (1)°. Half of the molecule is found in one asymmetric unit, related to the other half by a center of symmetry.

Table VII. Bond Angles (deg)[a] for $[Ph_4As]_2[Au_2(i\text{-}MNT)_2Cl_2]$ (**2**)

S(1)–Au–Cl	84.3 (1)	S(1)–Au–Au(a)	95.6 (1)
Cl–Au–Au(a)	178.7 (1)	S(1)–Au–S(2a)	168.3 (1)
Cl–Au–S(2a)	84.1 (1)	Au(a)–Au–S(2a)	96.0 (1)
C(11)–As–C(21)	109.3 (3)	C(11)–As–C(31)	107.3 (4)
C(21)–As–C(31)	112.1 (3)	C(11)–As–C(41)	109.2 (3)
C(21)–As–C(41)	109.0 (3)	C(31)–As–C(41)	109.9 (3)
Au–S(1)–C(1)	112.2 (2)	C(1)–S(2)–Au(a)	112.1 (3)
S(1)–C(1)–S(2)	124.0 (4)	S(1)–C(1)–C(2)	117.7 (6)
S(2)–C(1)–C(2)	118.3 (6)	C(1)–C(2)–C(3)	121.2 (7)
C(1)–C(2)–C(4)	121.5 (8)	C(3)–C(2)–C(4)	117.3 (7)
C(2)–C(3)–N(1)	177.8 (11)	C(2)–C(4)–N(2)	177.4 (10)
As–C(11)–C(12)	118.2 (6)	As–C(11)–C(16)	120.9 (6)
C(12)–C(11)–C(16)	120.9 (9)	C(11)–C(12)–C(13)	118.8 (7)
C(12)–C(13)–C(14)	120.0 (9)	C(13)–C(14)–C(15)	120.3 (11)
C(14)–C(15)–C(16)	121.5 (8)	C(11)–C(16)–C(15)	118.5 (7)
As–C(21)–C(22)	120.5 (5)	As–C(21)–C(26)	119.7 (6)
C(22)–C(21)–C(26)	119.7 (6)	C(21)–C(22)–C(23)	120.1 (7)
C(22)–C(23)–C(24)	120.3 (9)	C(23)–C(24)–C(25)	120.5 (7)
C(24)–C(25)–C(26)	119.8 (8)	C(21)–C(26)–C(25)	119.4 (9)
As–C(31)–C(32)	120.1 (6)	As–C(31)–C(36)	119.7 (6)
C(32)–C(31)–C(36)	120.1 (8)	C(31)–C(32)–C(33)	119.1 (9)
C(32)–C(33)–C(34)	121.0 (11)	C(33)–C(34)–C(35)	118.8 (11)
C(34)–C(35)–C(36)	119.9 (13)	C(31)–C(36)–C(35)	121.0 (10)
As–C(41)–C(42)	118.8 (5)	As–C(41)–C(46)	120.2 (6)
C(42)–C(41)–C(46)	120.9 (7)	C(41)–C(42)–C(43)	119.6 (8)
C(42)–C(43)–C(44)	118.6 (10)	C(43)–C(44)–C(45)	121.6 (8)
C(44)–C(45)–C(46)	119.9 (8)	C(41)–C(46)–C(45)	119.3 (8)

[a] Estimated standard deviations in the least significant digits are given in parentheses.

Table VIII. Atomic Coordinates ($\times 10^4$) and Isotropic Thermal Parameters ($Å^2 \times 10^3$)[a] for $[n\text{-}Bu_4N]_2[Au_2(i\text{-}MNT)_2Br_2]$ (**3**)

atom	x	y	z	U_{iso}[b]
Au(1)	4918 (1)	274 (2)	532 (1)	44 (1)*
Br(1)	4771 (3)	705 (9)	1589 (3)	92 (4)*
S(1)	5639 (5)	−338 (18)	1302 (6)	67 (7)*
S(2)	4179 (5)	1076 (19)	−45 (7)	64 (7)*
N	3665 (13)	3726 (47)	1842 (19)	55 (20)*
N(1)	6976 (20)	−2756 (62)	866 (25)	106 (34)*
N(2)	6693 (13)	−1526 (48)	2636 (19)	56 (20)*
C(1)	5983 (14)	−1078 (46)	920 (18)	29 (10)
C(2)	6396 (14)	−1557 (45)	1324 (19)	29 (10)
C(3)	6715 (20)	−2235 (63)	1060 (27)	64 (15)
C(4)	6580 (18)	−1500 (58)	2061 (27)	54 (14)
C(11)	3603 (15)	2024 (50)	1522 (21)	38 (12)
C(12)	3157 (17)	1729 (54)	942 (22)	53 (13)
C(13)	3146 (20)	16 (56)	627 (25)	68 (16)
C(14)	2695 (21)	−446 (67)	57 (28)	81 (17)
C(21)	3578 (17)	5054 (50)	1243 (22)	52 (13)
C(22)	3918 (19)	4897 (55)	895 (25)	63 (15)
C(23)	3778 (19)	6265 (65)	341 (26)	76 (17)
C(24)	4051 (24)	6209 (78)	−79 (32)	98 (21)
C(31)	4099 (20)	3849 (63)	2320 (26)	67 (15)
C(32)	4299 (24)	5503 (76)	2670 (30)	102 (21)
C(33)	4749 (21)	5359 (71)	3305 (30)	87 (18)
C(34)	4688 (25)	4773 (69)	3931 (31)	91 (19)
C(41)	3273 (17)	4154 (54)	2061 (23)	51 (13)
C(42)	3297 (17)	3112 (56)	2666 (23)	53 (13)
C(43)	2915 (19)	3580 (66)	2862 (26)	77 (17)
C(44)	2890 (21)	2435 (68)	3422 (27)	78 (17)

[a] Estimated standard deviations in the least significant digits are given in parentheses. [b] For values with asterisks, the equivalent isotropic U is defined as one-third of the trace of the $\mathbf{U}_{ij}$ tensor.

Table IX. Bond Lengths (Å)[a] for $[n\text{-}Bu_4N]_2[Au_2(i\text{-}MNT)_2Br_2]$ (**3**)

Au(1)–Br(1)	2.510 (8)	Au(1)–S(1)	2.303 (13)
Au(1)–S(2)	2.294 (13)	Au(1)–Au(1a)	2.570 (5)
S(1)–C(1)	1.725 (51)	S(2)–C(1a)	1.729 (41)
N–C(11)	1.523 (56)	N–C(21)	1.613 (60)
N–C(31)	1.366 (59)	N–C(41)	1.550 (76)
N(1)–C(3)	1.157 (96)	N(2)–C(4)	1.135 (69)
C(1)–C(2)	1.322 (51)	C(1)–S(2a)	1.729 (41)
C(2)–C(3)	1.461 (85)	C(2)–C(4)	1.446 (65)
C(11)–C(12)	1.495 (55)	C(12)–C(13)	1.544 (66)
C(13)–C(14)	1.524 (70)	C(21)–C(22)	1.553 (91)
C(22)–C(23)	1.557 (70)	C(23)–C(24)	1.486 (110)
C(31)–C(32)	1.551 (78)	C(32)–C(33)	1.547 (76)
C(33)–C(34)	1.505 (104)	C(41)–C(42)	1.523 (71)
C(42)–C(43)	1.499 (91)	C(43)–C(44)	1.545 (86)

[a] Estimated standard deviations in the least significant digits are given in parentheses.

Table X. Bond Angles (deg)[a] for $[n\text{-}Bu_4N]_2[Au_2(i\text{-}MNT)_2Br_2]$ (**3**)

Br(1)–Au(1)–S(1)	83.4 (4)	Br(1)–Au(1)–S(2)	85.3 (4)
S(1)–Au(1)–S(2)	168.4 (6)	Br(1)–Au(1)–Au(1a)	177.8 (2)
S(1)–Au(1)–Au(1a)	95.2 (4)	S(2)–Au(1)–Au(1a)	96.2 (4)
Au(1)–S(1)–C(1)	113.1 (12)	Au(1)–S(2)–C(1a)	112.6 (17)
C(11)–N–C(21)	107.8 (33)	C(11)–N–C(31)	108.4 (37)
C(21)–N–C(31)	110.3 (40)	C(11)–N–C(41)	111.3 (36)
C(21)–N–C(41)	100.6 (33)	C(31)–N–C(41)	118.0 (43)
S(1)–C(1)–C(2)	117.5 (33)	S(1)–C(1)–S(2a)	122.4 (22)
C(2)–C(1)–S(2a)	119.9 (38)	C(1)–C(2)–C(3)	122.5 (39)
C(1)–C(2)–C(4)	124.7 (48)	C(3)–C(2)–C(4)	112.8 (39)
N(1)–C(3)–C(2)	178.3 (58)	N(2)–C(4)–C(2)	174.4 (43)
N–C(11)–C(12)	115.5 (34)	C(11)–C(12)–C(13)	110.8 (39)
C(12)–C(13)–C(14)	114.9 (44)	N–C(21)–C(22)	113.1 (36)
C(21)–C(22)–C(23)	105.1 (43)	C(22)–C(23)–C(24)	112.1 (49)
N–C(31)–C(32)	121.8 (46)	C(31)–C(32)–C(33)	114.8 (48)
C(32)–C(33)–C(34)	113.3 (61)	N–C(41)–C(42)	111.0 (37)
C(41)–C(42)–C(43)	109.1 (40)	C(42)–C(43)–C(44)	111.4 (45)

[a] Estimated standard deviations in the least significant digits are given in parentheses.

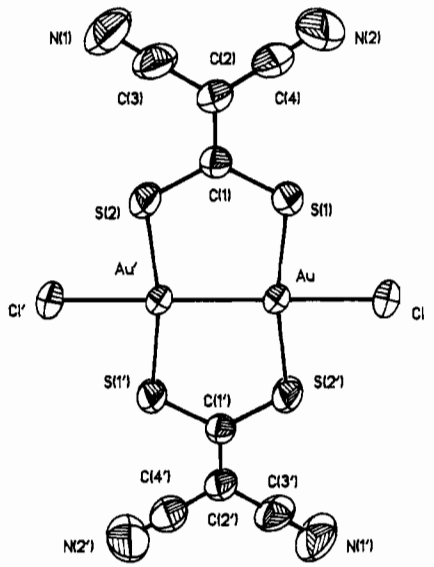

Figure 2. ORTEP drawing of the molecular structure and labeling scheme for the anion portions of compound **2**. Cation portions are omitted for clarity.

The most interesting feature in this molecule is the unusually short Au–Au distance, 2.796 (1) Å, significantly shorter than the distance observed in metallic gold[18] (2.884 Å). Similarly short Au–Au distances have been observed in dialkyldithiocarbamate-bridged Au^I dimers (2.76–2.79 Å).[5a,b] The bonding in **1a** is very similar to that in the dithiocarbamate-bridged Au^I dimer,[19] except that the dithiocarbamate-bridged Au^I dimer is twisted[5a,b] from planarity.

The anion portions of compounds **2** and **3** are shown in Figures 2 and 3, respectively. They are very much alike. The two *i*-MNT ligands bridge the two gold atoms similarly as found in **1a**, Au–

(18) Pearson, W. D. *Lattice Spacing and Structure of Metal and Alloys*; Pergamon Press: London, 1957.

(19) Farrel, F. J.; Spiro, T. G. *Inorg. Chem.* **1971**, *10*, 1606. The Au–Au stretch reported in this paper appears to be assigned incorrectly, however.[23]

Table XI. Atomic Coordinates ($\times 10^4$) and Isotropic Thermal Parameters ($Å^2 \times 10^3$)[a] for $[n\text{-}Bu_4N][Au(i\text{-}MNT)_2]$ (**4**)

atom	x	y	z	U_{iso}[b]
Au(1)	−63 (1)	1129 (1)	9458 (1)	51 (1)*
Au(2)	9920 (1)	3802 (1)	8235 (1)	52 (1)*
S(1)	−392 (2)	937 (2)	7787 (2)	61 (2)*
S(2)	−1803 (2)	1229 (2)	9012 (2)	63 (2)*
S(3)	1667 (3)	1029 (2)	9870 (2)	67 (2)*
S(4)	321 (2)	1280 (2)	11142 (2)	63 (2)*
S(5)	11458 (3)	4073 (2)	8661 (2)	68 (2)*
S(6)	10445 (3)	3644 (3)	9913 (2)	73 (2)*
S(7)	9394 (2)	3931 (2)	6539 (2)	61 (2)*
S(8)	8441 (3)	3455 (2)	7819 (2)	65 (2)*
C(1)	−1654 (9)	1045 (7)	7827 (8)	56 (3)
C(2)	−2388 (8)	985 (7)	7058 (8)	52 (3)
C(3)	−2175 (9)	854 (7)	6121 (8)	60 (3)
C(4)	−3412 (10)	1092 (8)	7120 (8)	62 (3)
C(5)	1569 (9)	1142 (7)	11073 (8)	54 (3)
C(6)	2360 (8)	1115 (7)	11821 (8)	52 (3)
C(7)	2261 (9)	1208 (7)	12809 (8)	61 (3)
C(8)	3332 (11)	1053 (9)	11668 (10)	89 (4)
C(9)	8403 (8)	3587 (7)	6617 (7)	47 (3)
C(10)	7700 (8)	3483 (7)	5837 (7)	50 (3)
C(11)	7663 (9)	3695 (7)	4873 (8)	59 (3)
C(12)	6923 (9)	3186 (7)	5950 (8)	59 (3)
C(13)	11540 (9)	3831 (7)	9848 (8)	59 (3)
C(14)	12353 (9)	3766 (8)	10612 (8)	64 (3)
C(15)	12346 (12)	3540 (10)	11555 (11)	101 (5)
C(16)	13253 (10)	3876 (8)	10541 (9)	74 (4)
C(21)	1667 (7)	3845 (6)	5056 (7)	38 (3)
C(22)	1237 (8)	3407 (7)	4184 (8)	60 (3)
C(23)	115 (9)	3973 (8)	3707 (9)	71 (4)
C(24)	−357 (11)	3595 (10)	2790 (10)	101 (5)
C(31)	2993 (8)	2414 (6)	5883 (7)	45 (3)
C(32)	2307 (8)	2391 (6)	6543 (7)	47 (3)
C(33)	2525 (8)	1435 (7)	6749 (8)	52 (3)
C(34)	1868 (9)	1383 (8)	7420 (8)	73 (4)
C(41)	3017 (7)	3869 (6)	6449 (7)	41 (3)
C(42)	4116 (8)	3511 (7)	7080 (7)	53 (3)
C(43)	4228 (10)	4134 (9)	7874 (9)	83 (4)
C(44)	5345 (11)	3843 (10)	8517 (11)	117 (6)
C(51)	3545 (8)	3206 (6)	4920 (7)	42 (3)
C(52)	3545 (8)	4027 (7)	4524 (7)	51 (3)
C(53)	4338 (8)	3776 (7)	3877 (7)	48 (3)
C(54)	4412 (10)	4528 (8)	3452 (9)	79 (4)
C(61)	6721 (8)	1243 (7)	1214 (7)	44 (3)
C(62)	5643 (8)	1672 (7)	543 (7)	54 (3)
C(63)	5479 (10)	1046 (8)	−242 (9)	77 (4)
C(64)	4388 (11)	1425 (9)	−884 (10)	102 (5)
C(71)	6803 (7)	2690 (6)	1818 (7)	40 (3)
C(72)	7471 (8)	2733 (6)	1145 (7)	44 (3)
C(73)	7251 (8)	3663 (7)	913 (7)	50 (3)
C(74)	7919 (9)	3707 (8)	258 (8)	73 (4)
C(81)	8092 (8)	1264 (7)	2613 (7)	46 (3)
C(82)	8529 (8)	1664 (7)	3516 (7)	47 (3)
C(83)	9662 (9)	1065 (7)	3986 (8)	61 (3)
C(84)	10098 (10)	1450 (9)	4904 (9)	88 (4)
C(91)	6223 (8)	1888 (6)	2763 (7)	44 (3)
C(92)	6237 (8)	1073 (7)	3168 (7)	52 (3)
C(93)	5480 (8)	1334 (7)	3820 (7)	50 (3)
C(94)	5369 (9)	582 (8)	4275 (8)	72 (4)
N(1)	2795 (6)	3335 (5)	5573 (5)	37 (2)
N(2)	6955 (6)	1769 (5)	2099 (5)	36 (2)
N(3)	−1979 (8)	765 (7)	5355 (7)	85 (3)
N(4)	−4227 (9)	1192 (7)	7180 (8)	86 (3)
N(7)	2220 (8)	1234 (7)	13609 (7)	80 (3)
N(8)	4141 (11)	939 (9)	11528 (9)	115 (4)
N(11)	7612 (8)	3886 (7)	4110 (7)	75 (3)
N(12)	6310 (8)	2945 (7)	6046 (8)	87 (3)
N(15)	12348 (12)	3340 (11)	12303 (11)	158 (6)
N(16)	13997 (9)	3981 (7)	10459 (8)	90 (4)

[a] Estimated standard deviations in the least significant digits are given in parentheses. [b] For values with asterisks, the equivalent isotropic U is defined as one-third of the trace of the U_{ij} tensor.

S(1) = 2.286 (2) Å, Au–S(2) = 2.287 (2) Å in **2** and Au–S(1) = 2.30 (1) Å, Au–S(2) = 2.29 (1) Å in **3**. However, the S(1)–Au–S(2)′ angles of 168.3 (1)° in **2** and 168.4 (6)° in **3** are considerably smaller than that in **1a** (172.2 (1)°). This is due to the Au–Au bond formation upon oxidation, Au–Au = 2.550 (1) Å in **2** and Au–Au = 2.570 (5) Å in **3**. These distances are ~0.22–0.24 Å shorter than that found in **1a**. The Au–Au bond, 2.550 (1) Å, is one of the shortest known Au–Au bonds.[3a,4a,b,7b,10b] The bond distances of halogen atoms and gold atoms are normal, Au–Cl = 2.380 (3) Å in **2** and Au–Br = 2.510 (8) Å in **3**. The ~3.0-Å separations between the sulfur atoms S(1) and S(2)′ in **1a**, **2**, and **3** indicate the presence of significant nonbonding interactions. Molecules of **2** and **3** also possess a center of symmetry and are nearly planar.

Table XII. Bond Lengths (Å)[a] for $[n\text{-}Bu_4N][Au(i\text{-}MNT)_2]$ (**4**)

Au(1)–S(1)	2.331 (3)	Au(1)–S(2)	2.343 (4)
Au(1)–S(3)	2.328 (4)	Au(1)–S(4)	2.340 (3)
Au(2)–S(5)	2.340 (4)	Au(2)–S(6)	2.321 (3)
Au(2)–S(7)	2.344 (3)	Au(2)–S(8)	2.332 (4)
S(1)–C(1)	1.747 (14)	S(2)–C(1)	1.738 (12)
S(3)–C(5)	1.739 (12)	S(4)–C(5)	1.724 (14)
S(5)–C(13)	1.731 (13)	S(6)–C(13)	1.731 (15)
S(7)–C(9)	1.751 (14)	S(8)–C(9)	1.724 (11)
C(1)–C(2)	1.346 (15)	C(2)–C(3)	1.418 (17)
C(2)–C(4)	1.420 (19)	C(3)–N(3)	1.173 (17)
C(4)–N(4)	1.128 (20)	C(5)–C(6)	1.337 (15)
C(6)–C(7)	1.435 (17)	C(6)–C(8)	1.414 (22)
C(7)–N(7)	1.149 (16)	C(8)–N(8)	1.155 (23)
C(9)–C(10)	1.355 (15)	C(10)–C(11)	1.424 (17)
C(10)–C(12)	1.423 (20)	C(11)–N(11)	1.131 (16)
C(12)–N(12)	1.136 (21)	C(13)–C(14)	1.356 (16)
C(14)–C(15)	1.421 (21)	C(14)–C(16)	1.393 (22)
C(15)–N(15)	1.138 (24)	C(16)–N(16)	1.173 (21)
C(21)–C(22)	1.517 (15)	C(21)–N(1)	1.508 (10)
C(22)–C(23)	1.506 (14)	C(23)–C(24)	1.529 (19)
C(31)–C(32)	1.522 (18)	C(31)–N(1)	1.527 (14)
C(32)–C(33)	1.536 (16)	C(33)–C(34)	1.515 (20)
C(41)–C(42)	1.504 (13)	C(41)–N(1)	1.520 (12)
C(42)–C(43)	1.500 (17)	C(43)–C(44)	1.532 (18)
C(51)–C(52)	1.520 (17)	C(51)–N(1)	1.521 (15)
C(52)–C(53)	1.537 (17)	C(53)–C(54)	1.483 (20)
C(61)–C(62)	1.515 (12)	C(61)–N(2)	1.526 (13)
C(62)–C(63)	1.511 (17)	C(63)–C(64)	1.503 (16)
C(71)–C(72)	1.527 (17)	C(71)–N(2)	1.534 (14)
C(72)–C(73)	1.501 (16)	C(73)–C(74)	1.507 (20)
C(81)–C(82)	1.515 (14)	C(81)–N(2)	1.515 (11)
C(82)–C(83)	1.529 (12)	C(83)–C(84)	1.518 (17)
C(91)–C(92)	1.508 (17)	C(91)–N(2)	1.514 (15)
C(92)–C(93)	1.502 (17)	C(93)–C(94)	1.532 (19)

[a] Estimated standard deviations in the least significant digits are given in parentheses.

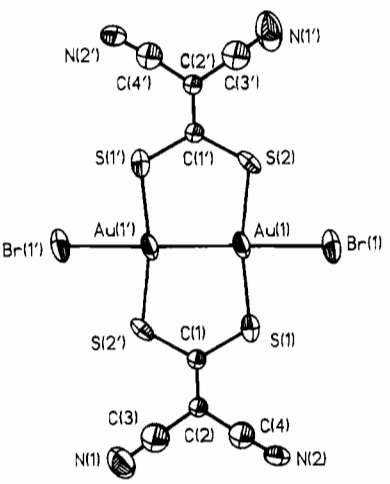

Figure 3. ORTEP drawing of the molecular structure and labeling scheme for the anion portions of compound **3**. Cation portions are omitted for clarity.

The molecular structure and labeling scheme for compound **4** is shown in Figure 4. The two independent molecules are essentially the same. The gold atom is surrounded by four sulfur atoms in an approximately planar arrangement, typical for

Table XIII. Bond Angles (deg)[a] for $[n\text{-}Bu_4N][Au(i\text{-}MNT)_2]$ (**4**)

S(1)-Au(1)-S(2)	74.9 (1)	S(1)-Au(1)-S(3)	104.0 (1)
S(2)-Au(1)-S(3)	178.9 (1)	S(1)-Au(1)-S(4)	178.1 (1)
S(2)-Au(1)-S(4)	106.4 (1)	S(3)-Au(1)-S(4)	74.7 (1)
S(5)-Au(2)-S(6)	74.8 (1)	S(5)-Au(2)-S(7)	105.7 (1)
S(6)-Au(2)-S(7)	178.8 (1)	S(5)-Au(2)-S(8)	177.1 (1)
S(6)-Au(2)-S(8)	104.7 (1)	S(7)-Au(2)-S(8)	74.7 (1)
Au(1)-S(1)-C(1)	87.9 (4)	Au(1)-S(2)-C(1)	87.8 (4)
Au(1)-S(3)-C(5)	87.7 (4)	Au(1)-S(4)-C(5)	87.7 (4)
Au(2)-S(5)-C(13)	87.3 (5)	Au(2)-S(6)-C(13)	87.9 (4)
Au(2)-S(7)-C(9)	87.3 (4)	Au(2)-S(8)-C(9)	88.3 (5)
S(1)-C(1)-S(2)	109.4 (6)	S(1)-C(1)-C(2)	125.0 (10)
S(2)-C(1)-C(2)	125.6 (11)	C(1)-C(2)-C(3)	120.0 (12)
C(1)-C(2)-C(4)	123.2 (11)	C(3)-C(2)-C(4)	116.8 (10)
C(2)-C(3)-N(3)	177.6 (16)	C(2)-C(4)-N(4)	178.5 (14)
S(3)-C(5)-S(4)	109.9 (6)	S(3)-C(5)-C(6)	124.1 (10)
S(4)-C(5)-C(6)	126.1 (10)	C(5)-C(6)-C(7)	123.1 (12)
C(5)-C(6)-C(8)	120.9 (12)	C(7)-C(6)-C(8)	115.9 (11)
C(6)-C(7)-N(7)	176.1 (11)	C(6)-C(8)-N(8)	175.0 (16)
S(7)-C(9)-S(8)	109.5 (6)	S(7)-C(9)-C(10)	123.8 (10)
S(8)-C(9)-C(10)	126.7 (11)	C(9)-C(10)-C(11)	122.6 (13)
C(9)-C(10)-C(12)	120.9 (11)	C(11)-C(10)-C(12)	116.5 (10)
C(10)-C(11)-N(11)	178.1 (11)	C(10)-C(12)-N(12)	179.4 (10)
S(5)-C(13)-S(6)	109.8 (6)	S(5)-C(13)-C(14)	125.5 (12)
S(6)-C(13)-C(14)	124.7 (11)	C(13)-C(14)-C(15)	120.6 (14)
C(13)-C(14)-C(16)	124.1 (13)	C(15)-C(14)-C(16)	115.3 (11)
C(14)-C(15)-N(15)	178.3 (17)	C(14)-C(16)-N(16)	178.3 (12)
C(22)-C(21)-N(1)	115.4 (7)	C(21)-C(22)-C(23)	111.5 (9)
C(22)-C(23)-C(24)	114.5 (10)	C(32)-C(31)-N(1)	113.9 (7)
C(31)-C(32)-C(33)	109.0 (8)	C(32)-C(33)-C(34)	110.6 (9)
C(42)-C(41)-N(1)	116.4 (7)	C(41)-C(42)-C(43)	110.0 (8)
C(42)-C(43)-C(44)	113.3 (10)	C(52)-C(51)-N(1)	116.8 (8)
C(51)-C(52)-C(53)	109.8 (8)	C(52)-C(53)-C(54)	114.7 (9)
C(62)-C(61)-N(2)	115.3 (7)	C(61)-C(62)-C(63)	109.6 (8)
C(62)-C(63)-C(64)	111.2 (9)	C(72)-C(71)-N(2)	115.8 (7)
C(71)-C(72)-C(73)	111.1 (8)	C(72)-C(73)-C(74)	111.2 (9)
C(82)-C(81)-N(2)	116.8 (7)	C(81)-C(82)-C(83)	111.2 (8)
C(82)-C(83)-C(84)	111.6 (9)	C(92)-C(91)-N(2)	117.3 (8)
C(91)-C(92)-C(93)	108.8 (8)	C(92)-C(93)-C(94)	115.9 (9)
C(21)-N(1)-C(31)	112.9 (8)	C(21)-N(1)-C(41)	105.6 (6)
C(31)-N(1)-C(41)	111.0 (7)	C(21)-N(1)-C(51)	111.4 (7)
C(31)-N(1)-C(51)	105.1 (7)	C(41)-N(1)-C(51)	111.0 (9)
C(61)-N(2)-C(71)	112.1 (7)	C(61)-N(2)-C(81)	106.4 (6)
C(71)-N(2)-C(81)	109.7 (8)	C(61)-N(2)-C(91)	111.2 (9)
C(71)-N(2)-C(91)	106.4 (7)	C(81)-N(2)-C(91)	111.0 (7)

[a] Estimated standard deviations in the least significant digits are given in parentheses.

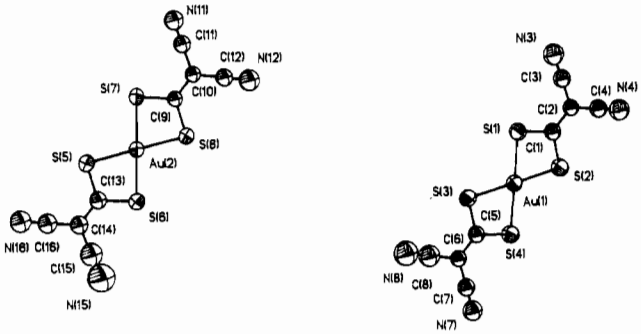

Figure 4. ORTEP drawing of the molecular structure and labeling scheme for the anion portions of compound **4**. Cation portions are omitted for clarity.

gold(III) complexes.[20] The maximum deviation from planarity is 0.02 Å in molecule 1 and 0.03 Å in molecule 2. The averaged Au–S distance of 2.335 (4) Å in **4** is much longer than those found in compound **1** (2.282 (2) Å), compound 2 (2.287 (2) Å), and compound **3** (2.29 (1) Å). The S–C distance, 1.74 (1) Å, on average is similar to that of compound **1a**, 1.731 (9) Å, but longer than the average S–C distance of 1.707 (8) Å in compound **2**.

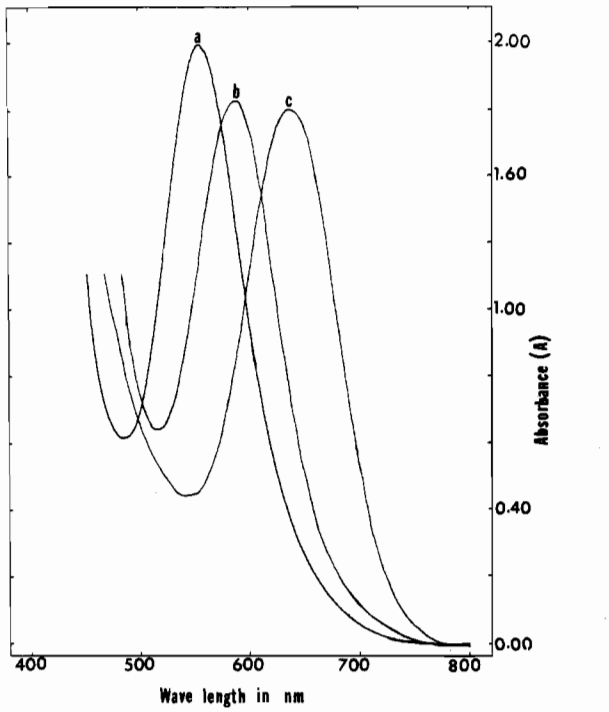

Figure 5. UV–visible absorption spectra: (a) $[Ph_4As]_2[Au_2(i\text{-}MNT)_2Cl_2]$ (**2**); (b) $[n\text{-}Bu_4N]_2[Au_2(i\text{-}MNT)_2Br_2]$ (**3**); (c) $[Ph_4As]_2[Au_2(i\text{-}MNT)_2I_2]$ (**5**).

In contrast, the C–C double-bond distance of 1.35 (1) Å in **4** is shorter than the C–C double-bond distance in **1a** (1.37 (1) Å) and in **2** (1.38 (1) Å). Similarly coordinated sulfur ligands in monomeric Au^{III} complexes have been observed previously.[8] The structures of the cation $n\text{-}Bu_4N^+$ in **1a**, **3**, and **4** are very similar. No disorder of the *n*-butyl groups was observed.

UV–Visible Spectral Studies. The visible spectra of the chloro (**2**), bromo (**3**), and iodo (**5**) complexes were obtained in the solvents CH_2Cl_2, THF, and CH_3CN at three different temperatures. In the case of the unstable iodo, complex, the visible spectra were recorded at temperatures lower than −5 °C. The chloro (**2**), bromo (**3**), and iodo (**5**) compounds showed strong absorption bands at 550 (18 181), 586 (17 064), and 640 nm (15 625 cm^{-1}), respectively. These three absorption bands are shown in Figure 5. They nicely follow (linearly) the ionization potential of the halogen.

The absorption bands may be assigned to low-energy electronic transitions that have a considerable σ–σ^* character. Fenske–Hall orbital calculations[21] on the anions of $[Au^{I}_2(i\text{-}MNT)_2]^{2-}$ and $[Au^{II}_2(i\text{-}MNT)_2X_2]^{2-}$ (X = Cl^-, Br^-, I^-) were performed. The orbitals involving metal atoms and the halide ligands are shown in the Figure 8. Significant contribution to the bonding from the 6s orbitals in $[Au^{I}_2(i\text{-}MNT)_2]^{2-}$ is apparent, but no net bonding is conclusive from this calculation. Both of the anions have an approximate D_{2h} symmetry. The energy gap, ΔE, between the filled A_{1g} (σ) orbital and the empty B_{2u} (σ^*) orbital in $[Au^{II}_2(i\text{-}MNT)_2X_2]^{2-}$ decreases with the decrease of the electronegativity of the X ligand, i.e., $Cl^- > Br^- > I^-$. This is consistent with the observed Au–Au bond lengths, 2.550 Å in $[Au^{II}_2(i\text{-}MNT)_2Cl_2]^{2-}$ vs 2.570 Å in $[Au^{II}_2(i\text{-}MNT)_2Br_2]^{2-}$, and the UV–vis absorption band of $[Au^{II}_2(i\text{-}MNT)_2X_2]^{2-}$ (550 nm, X = Cl; 586 nm, X = Br; 640 nm, X = I. Hence, the UV–vis absorption band is assigned to the σ–σ^* transition.

The absorption bands for all three systems were found to be insensitive to different solvent systems. No significant shift is observed, even with a strong base solvent such as pyridine. This observation is also supporting evidence for the σ–σ^* transition

(20) (a) Chiari, B.; Piovesance, O.; Tarantelli, T.; Zanazzi, P. F. *Inorg. Chem.* **1985**, *24*, 366. (b) Beurskens, P. T.; Vander Linden, J. Q. M. *Inorg. Chem.* **1970**, *9*, 475.

(21) Due to the instability of $[Au_2(i\text{-}MNT)_2I_2]^{2-}$, no crystal structure data were available. The calculation was performed by using the reported bond lengths of Au^{II}–I and Au^{II}–Au^{II} of the analogous compounds in the literature.

Table XIV. Rate Constants and Activation Energies for the Disproportionation of the Halide Complexes

complex (C)	[C], M	T, K	$1/T$	k, s^{-1}	log k	ϵ, cm^{-1} mol^{-1}
2	5.0×10^{-4}	293	0.003 41	2.20×10^{-4}	−3.18	2800
	5.0×10^{-4}	298	0.003 35	4.32×10^{-4}	−3.36	2980
	5.0×10^{-4}	303	0.003 30	6.58×10^{-4}	−3.65	2360
			E_a = 21.06 kcal/mol, abs at 550 nm			
3	5.0×10^{-4}	288	0.003 47	6.14×10^{-4}	−3.21	3600
	5.0×10^{-4}	293	0.003 41	1.10×10^{-3}	−2.95	3480
	5.0×10^{-4}	298	0.003 35	1.80×10^{-3}	−2.73	3440
			E_a = 18.42 kcal/mol, abs at 586 nm			
5	3.5×10^{-4}	253	0.003 95	2.61×10^{-4}	−3.58	5514
	3.5×10^{-4}	258	0.003 87	6.53×10^{-4}	−3.18	3771
	3.5×10^{-4}	263	0.003 80	1.33×10^{-3}	−2.87	2514
			E_a = 10.5 kcal/mol, abs at 640 nm			

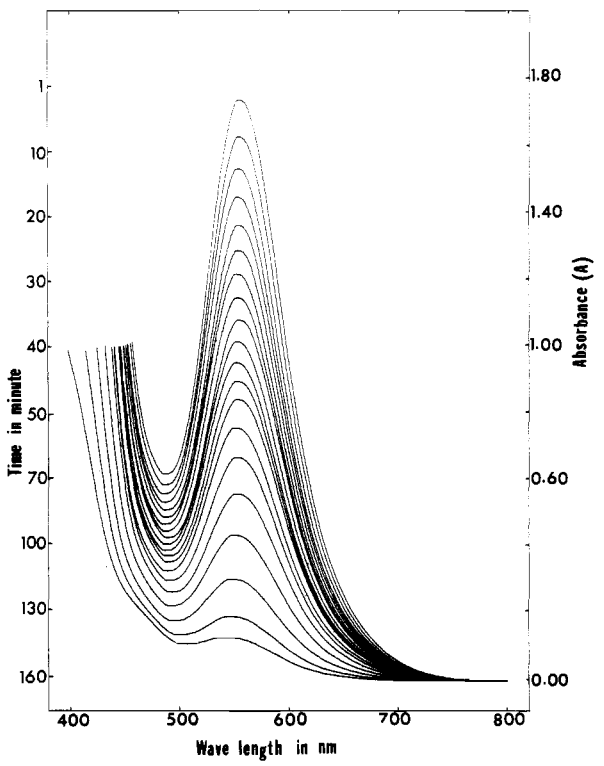

Figure 6. UV–visible spectra for the gradual change of the absorbance of the gold dimer $[Ph_4As]_2[Au_2(i\text{-}MNT)_2Cl_2]$, initially $\sim 5 \times 10^{-4}$ M, as a function of decomposition with time.

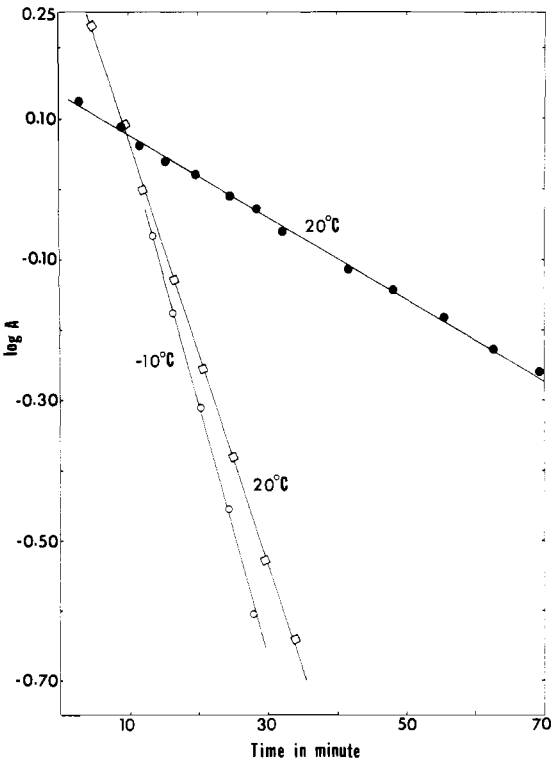

Figure 7. Plot of log A (absorbance) versus t (time: (●) $[Ph_4As]_2[Au_2(i\text{-}MNT)_2Cl_2]$ (**2**); (□) $[n\text{-}Bu_4N]_2[Au_2(i\text{-}MNT)_2Br_2]$ (**3**); (○) $[Ph_4As]_2[Au_2(i\text{-}MNT)_2I_2]$ (**5**).

assignment. The complexes are structurally similar to the gold(II) ylide dimers, but a low-energy (visible) electronic transition has not been observed in the ylide complexes. In the case of the gold(II) ylide dimer, it has been reported[22] from a ASED calculation that the dichloride adduct of the gold(II) ylide is more stable than those of the dibromide and diiodide. This trend of stability was explained[22] on the basis of the HOMO–LUMO separation stemming from the differences in the electronegativity of the halides. The electronegativity of chloride is greater than that of the other two halogens, thus the dichloride gold(II) ylide dimer forms a stronger metal–metal bond. With *i*-MNT the Cl complex also forms a metal–metal bond stronger than those of the other halogen complexes studied.

The decomposition of the $[Au_2(i\text{-}MNT)_2X_2]^{2-}$ complexes was monitored by recording the absorbance (A) with time, as shown in Figure 6. A plot of the log of absorbance versus time (t) gives a straight line for the systems studied at all temperatures, as is shown in Figure 7. This indicates that the decomposition occurs via pseudo-first-order kinetics. The rate constants were obtained from the slopes.

Table XV. Data for the Effect of Halide Ions and Solvents on the Rate of Disproportionation Reactions

$10^3[X^-]$, M[a]	10^4k_{obs}, s^{-1} [b]	$10^3[X^-]$, M[a]	10^4k_{obs}, s^{-1} [b]
3.75	6.30	28.10	21.00
7.14	8.67	37.50	28.00
11.20	10.40	46.80	32.35
18.70	16.20	56.20	38.60

solvents	k_1[complex][S], s^{-1} [c]	solvents	k_1[complex][S], s^{-1} [c]
CH_2Cl_2	3.26×10^{-4}	THF	3.80×10^{-4}
CH_3CN	3.89×10^{-4}	CH_2Cl_2/py	2.89×10^{-3}

[a] X^- = Cl; $[Y^+]_2[Au(i\text{-}MNT)X]_2 = 3.75 \times 10^{-4}$ M; temperature 25 °C. [b] $k_{obs} = \{k_1[complex][S] + k_2[complex][X]\}$ s^{-1}; S = solvent. [c] $[Y^+]_2[Au(i\text{-}MNT)X]_2 = 3.30 \times 10^{-4}$ M; temperature 25 °C.

The rate constants presented in Table XIV demonstrate that the decomposition in the case of the iodo complex is much faster than in the other two systems, a result consistent with the information described above. The activation energies (Table XIV) of the three systems were determined from the slope of the linear plot of log k_{obs} versus $1/T$, as is shown in Figure 9. The trend

(22) Bancroft, B. T. Ph.D. Thesis, 1984, p 177.
(23) Clark, R. J. H.; Tocher, J. H.; Fackler, J. P., Jr.; Neira, R.; Murray, H. H.; Knachel, H. *J. Organomet. Chem.* **1986**, *303*, 437.

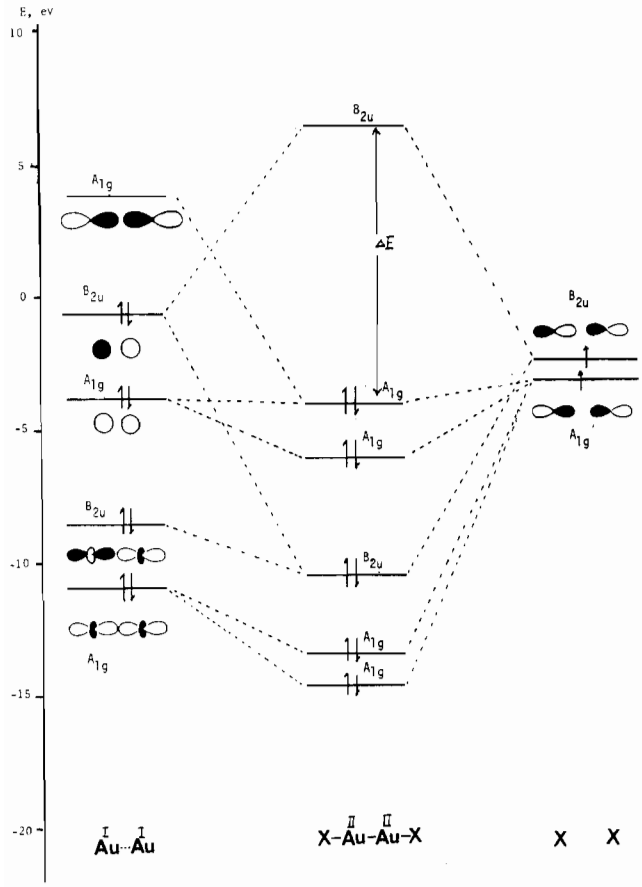

Figure 8. Orbital energy diagram for the anions of $[Au^{I}_2(i\text{-}MNT)_2]^{2-}$ and $[Au^{II}_2(i\text{-}MNT)_2X_2]^{2-}$ obtained from the Fenske–Hall orbital calculations.

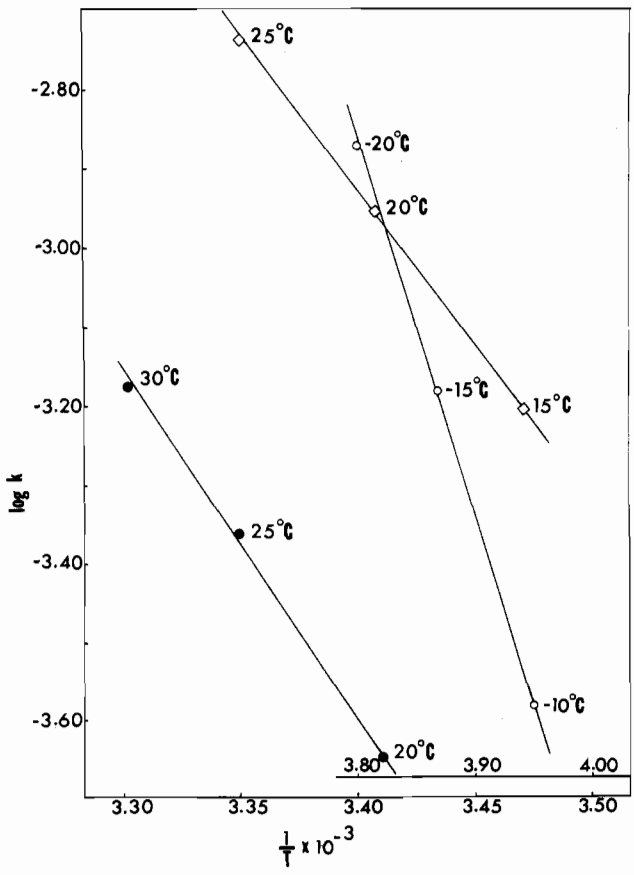

Figure 9. Plot of log k (rate constants) versus $1/T$: (●) $[Ph_4As]_2[Au_2(i\text{-}MNT)_2Cl_2]$ (**2**); (□) $[n\text{-}Bu_4N]_2[Au_2(i\text{-}MNT)_2Br_2]$ (**3**); (○) $[Ph_4As]_2[Au_2(i\text{-}MNT)_2I_2]$ (**5**).

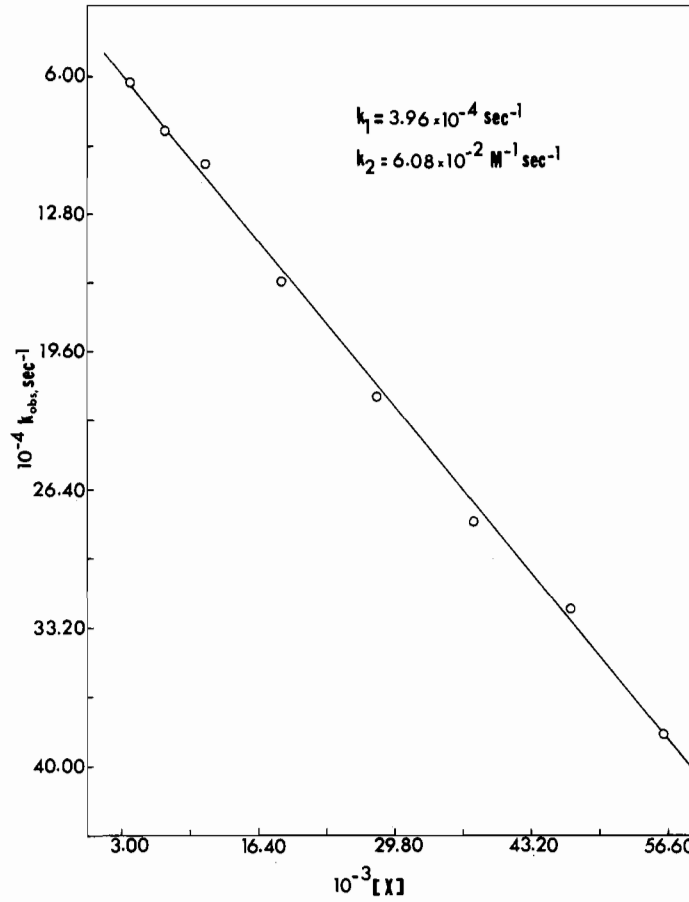

Figure 10. Plot of k_{obs} (rate constants) versus $[X^-]$ for complex **2**.

in activation energies, $E_a(Cl) > E_a(Br) \gg E_a(I)$, also provides further evidence for formation of the strongest metal–metal bond in the case of chloro dimer.

The rate of disproportionation has been found to depend on the presence of excess halide ions as well as with coordinating solvents. The rate of disproportionation gradually increases with increasing halide ion concentration at each temperature.

The rate of disproportionation (k_{obs}) has been obtained at a number of different Cl^- concentrations (keeping the metal concentration constant). A straight line resulted for each concentration when log A (absorbance) versus time was plotted (Figure 10). In this way several k_{obs} were obtained from the slopes. These results (Table XV) were used to determine the individual rate constants for k_1 (solvent-dependent path) and k_2 (halide ion dependent path) according to the following equation:[24] $k_{obs} = k_1[\text{complex}][S] + k_2[\text{complex}][X]$, where S = solvent and X = halide ions. In the absence of excess halide the solvent-dependent term dominates the kinetics. The agreement between the k_1 obtained (Figure 10) for the chloride complex at 25 °C and the pseudo-first-order rate constant (Table XIV) confirms this point.

The solvent dependency was demonstrated by several experiments. It was observed that the rate of disproportionation in weakly coordinating solvent systems such as THF, CH_3CN, and CH_2Cl_2 remained almost constant but the rate dramatically increased when two drops of pyridine were added to the CH_2Cl_2 solution. Since halide ions as well as solvents have significant influence on the rate of disproportionation, the rate-determining step involves association of a halide ion or solvent. Similar associative mechanisms are very common in the case of ligand-substitution reactions of square-planar mononuclear d^8 systems.[24]

The similarity between the disproportionation reaction of the dimer $[Au(i\text{-}MNT)X]_2^{2-}$ and mononuclear square-planar d^8 complexes is significant and suggests that nucleophilic attack at

(24) Basolo, F.; Pearson, R. G. *Mechanisms of Inorganic Reactions. A Study of Metal Complexes in Solution*; John Wiley and Sons, Inc.: New York, 1967; p 378.

Scheme I

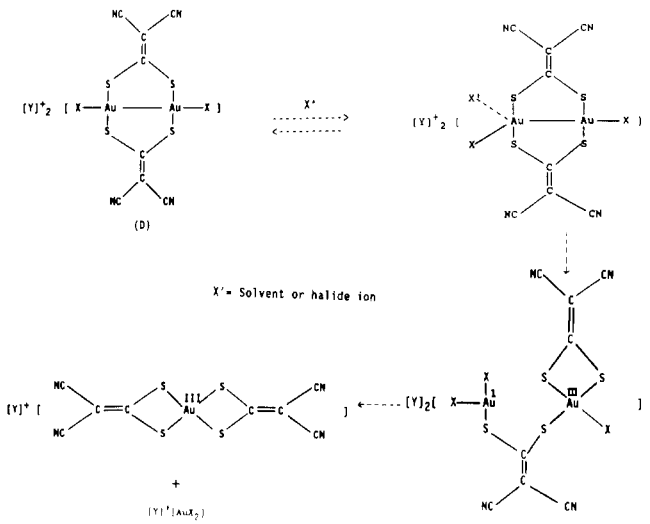

the gold center destabilizes the dimer. With the gold(II) ylide complex, $Au_2(ylide)_2Cl_2$, ligand rearrangement occurs[9c,22] in an ionizing solvent to form the mixed-valent Au^{III}/Au^{I} species Cl-(ylide)Au^{III}(ylide)Au^{I}Cl. Rupture of the Au–Au bond is required. Thus, a nucleophilic solvent, or nucleophiles in general, appear to destabilize the metal–metal bond in these d^9–d^9 dimer systems.

Stated differently, the important step in the homovalent Au^{II}_2 to the hetervalent Au^{III}/Au^{I} rearrangement is an association of either halide ions or a solvent molecule to form a 5-coordinate Au^{II} center, as is shown in Scheme I. Rupture of the metal–metal bond and a metal–ligand bond allows rearrangement of the molecule to a 3-coordinate Au^{I} and a 4-coordinate Au^{III} center via ligand addition to the latter. The formation of 3-coordinate Au^{I} and 4-coordinate planar Au^{III} is very common.[23,16] The labile sulfur compounds further rearrange to stable mononuclear planar Au^{III} and linear Au^{I} species.

In summary, strong σ-donor ligands support the electrophilic excitation of the d^{10} configuration to a d^9s^1 configuration, thus forming a stable metal–metal-bonded Au^{II} system with oxidative addition across the two metal atoms. In this *i*-MNT system the dianionic nature of the ligand coordinated through the sulfur atoms supplies sufficient electron density through σ donation to the Au^{I} centers to form a stable Au^{II} product. The stability of the Au^{II} product is dependent on the nature of halogen used as an oxidant. The rate of disproportionation of $[Y^+]_2[Au_2(i\text{-}MNT)_2X_2]$ is dependent on halide ion concentration as well as coordinating solvents. Decomposition occurs by a pseudo-first-order reaction pathway in the absence of excess halide.

Acknowledgment. This work has been supported by the National Science Foundation (Grant CHE 8708725), the Robert A. Welch Foundation, and the Texas A&M University Available Fund.

Supplementary Material Available: For **1a–4**, listings of crystallographic data, anisotropic thermal parameters, H atom coordinates, and isotropic thermal parameters (11 pages); tables of F_o, F_c, and $\sigma(F)$ (119 pages). Ordering information is given on any current masthead page.

Contribution from the Departments of Chemistry, Faculty of Engineering Science, Osaka University, Toyonaka, Osaka 560, Japan, and Faculty of Science, Yamagata University, Yamagata 990, Japan

Synthesis, Structure, and Electronic Properties of Octakis(μ_3-sulfido)hexakis(triethylphosphine)hexatungsten as a Tungsten Analogue of the Molecular Model for Superconducting Chevrel Phases

Taro Saito,*,† Akihiko Yoshikawa,† Tsuneaki Yamagata,† Hideo Imoto,† and Kei Unoura‡

Received February 3, 1989

The hexanuclear tungsten complex $[W_6S_8(PEt_3)_6]$ was synthesized by the reaction of magnesium metal on a trinuclear tungsten chloro sulfido cluster compound prepared from W_6Cl_{12}, elemental sulfur, and triethylphosphine. The complex crystallizes in the triclinic space group $P\bar{1}$ with a = 20.509 (5) Å, b = 12.905 (3) Å, c = 12.051 (3) Å, α = 108.51 (2)°, β = 92.41 (2)°, γ = 89.22 (3)°, and Z = 2. A unit cell contains two independent and nearly identical cluster units A and B. The cluster skeleton is a regular octahedron of six tungsten atoms coordinated with μ_3-sulfido ligands on each triangular face and triethylphosphine on each metal vertex. The structure is almost identical with that of the molybdenum analogue, but the electronic spectra (λ_{max} (ϵ) 409 (8.7 × 10^3), 882 (2.5 × 10^3), 964 (sh)) and the one-electron-oxidation (−0.46 V) and -reduction (−1.83 V) potentials vs the ferrocene/ferrocenium (Fc/Fc^+) redox couple in CH_2Cl_2 are significantly different. The difference is discussed in terms of the electronic levels of the W_6S_8 framework, which may be regarded as the cluster core of the unknown tungsten analogues of the Chevrel phases.

Introduction

The superconducting Chevrel phases $M_xMo_6X_8$ (M = Pb, Sn, Cu, etc.; X = S, Se, Te) have been extensively studied,[1] but no tungsten analogue has been reported. It would be very useful to have evidence for the stability of the W_6X_8 cluster framework before starting synthetic efforts on "tungsten Chevrels", and also the electronic properties of the molecular W_6X_8 cluster would give us a clue to the properties of the still unknown solid-state $M_xW_6X_8$ compounds. We report here the synthesis of $[W_6S_8(PEt_3)_6]$ as the second example of reductive dimerization of trinuclear sulfido complexes to form an octahedral cluster.[2] As the potential starting compound $W_3S_7Cl_4$ had not been reported, we first tried to prepare it from tungsten dichloride.[3]

Experimental Section

Reagents. W_6Cl_{12}[4] was prepared by treating $(H_3O)_2[W_6Cl_{14}]\cdot 6H_2O$ under vacuum at 230 °C for 2 h. PEt_3 (21.6% in toluene, Nippon Chemical Co. Ltd.) was used as received. The solvents were dried and distilled under dinitrogen.

Instruments. Infrared spectra were recorded by a Hitachi 295 instrument (4000–250 cm^{-1}). UV-vis spectra were obtained by Simadzu UV-265FS (300–900 nm) and Hitachi U-3400 (900–2000 nm) spectrophotometers. XPS spectra were measured by a VG Scientific Escalab

* To whom correspondence should be addressed at the Department of Chemistry, Faculty of Science, The University of Tokyo, Hongo, Tokyo 113, Japan.
† Osaka University.
‡ Yamagata University.

(1) *Superconductivity in Ternary Compounds I*; Fischer, Ø., Maple, M. B., Eds.; Springer-Verlag: Berlin, 1982.
(2) Saito, T.; Yamamoto, N.; Yamagata, T.; Imoto, H. *J. Am. Chem. Soc.* **1988**, *110*, 1646.
(3) Opalovskii, A. A.; Federov, V. E.; Mazhara, A. P.; Chermisina, I. M. *Zh. Neorg. Khim.* **1972**, *17*, 2876.
(4) Schäfer, H.; Trenkel, M.; Brendel, C. *Monatsh. Chem.* **1971**, *102*, 1293.

0020-1669/89/1328-3588$01.50/0